Hindawi
Complexity
Volume 2021, Article ID 9162259, 13 pages
https://doi.org/10.1155/2021/9162259

Research Article

Fast Simulation and Chaos Investigation of a DC-DC Boost Inverter

Rachid Dhifaou[1] **and Houda Brahmi**[2]

[1]*Unit of Research (ERCO), INSAT Tunisia, Centre Urbain Nord, B.P. N 676, 1080 Tunis Cedex, Tunisia*
[2]*University of Tunis el Manar, Higher Institute of Medicals Technologies of Tunis (ISTMT), Unit of Research ERCO-INSAT, 9 Rue Zouhair Essafi, 1006 Tunis, Tunisia*

Correspondence should be addressed to Houda Brahmi; houda.brahmi@istmt.utm.tn

Received 24 May 2021; Accepted 29 July 2021; Published 14 August 2021

Academic Editor: Guillermo Huerta Cuellar

Intensive and repetitive simulations are required to study static and dynamic behaviours of systems. Particular phenomena such as bifurcation and chaos require long simulation times and analysis. To check the existence of bifurcations and chaos in a dynamic system, a fine-tuning procedure of a bifurcation parameter is to be carried out. This increases considerably the computing time, and a great amount of patience is needed to obtain adequate results. Because of the high switching frequency of a boost inverter, the integration process of the dynamic model used to describe it uses an integration step that is in general less than one microsecond. This makes the integration process time consuming even for a short simulation. Thus, a fast, but accurate, method is suitable to analyse the dynamic behaviour of the converter. This work contains two topics. First, we develop a like-discrete integration process that permits precise results in a very fast manner. For one switching period, we compute only two or a maximum of three breaking points depending on whether we treat a continuous conduction mode (CCM) or a discontinuous conduction mode (DCM) of the inductor current. Furthermore, with each segment of the dynamic trajectory, an exact analytic formula is associated. The second goal is to use this result to develop a discrete iterative map formulated as in standard discrete time series models. The Jacobian matrix of the found iterative map is defined and used to compute Lyapunov exponents to prove existence of chaos. Performance of the developed study is positively evaluated by using classical simulations and fine-tuning a bifurcation parameter to detect chaos. This parameter is the desired reference of the inductor current peak. Results show that the proposed scheme is very fast and accurate. The study can be easily extended to other switching topologies of DC-DC inverters.

1. Introduction

DC-DC boost inverter, also known as a step up inverters, are largely studied in literature [1–3]. These power electronic devices transfer electric energy from a DC input voltage source to an output load that requires a higher voltage. The efficiency of DC-DC boost inverter is good in general which makes them largely employed in various applications. Battery chargers, photovoltaic energy-based systems, and DC motor drives are typical examples [4,5]. As for all DC-DC power converter topologies, energy transfer in this device is achieved by switching the state of a power transistor at high frequencies. Output voltage or current is varied by adjusting the control variable, commonly named the duty cycle. The operating steady-state regime can be done with an open loop or closed loop configuration, by using the appropriate controller. Important advances are reached in the field of both voltage control and current control [6–8].

To perform successful and reliable practical control, numerical simulations are of great importance. Intensive and repetitive simulations are also needed to study particular phenomena such as bifurcations [9,10] and chaos [10,11]. It is shown in the literature that a lot of piecewise dynamic systems exhibit chaotic behaviour [12,13]. DC-DC converters are nonlinear periodically controlled systems that operate under practically piecewise dynamic trajectories. Chaotic regimes are confirmed for various switching power converters.

To check the existence of bifurcations and chaos in a dynamic system, a fine-tuning procedure of a bifurcation parameter is required. This increases considerably the computing time, and a great amount of patience is required to establish adequate results. Because of the high switching frequency of the PWM technique [14], to solve the model of a DC-DC boost inverter, an integration step smaller than one microsecond is required. This makes the integration process time consuming even for short simulations. Thus, a fast, but accurate, method is required to analyse the dynamic behaviour of the converter.

The first goal of this work is to develop a type-like discrete integration process with precise and fast results. For one switching period, we compute only two or a maximum of three breaking points depending on whether we treat a continuous conduction mode (CCM) or a discontinuous conduction mode (DCM) of the inductor current [1,2]. Furthermore, with each segment of the dynamic trajectory, an exact analytic formula is associated.

The second goal of the paper is to use these results in developing a discrete iterative map formulated as in standard discrete time series models [15,16]. A Jacobian matrix as found with an iterative map is defined and used to compute Lyapunov exponents [12,13] via the QR factorisation technique.

In switching inverter topologies, a current peak control (CPC) is frequently used [3] to impose an adequate operating point. In such case, the feedback control block is composed of a saw tooth generator, a comparator, and a latch. A drive circuit uses latch output to generate the gating pulses. The switch is turned on at the beginning of each switching period and turned off if the inductor current becomes greater than a reference value and remains in the off state until the beginning of the next cycle. Simulations of this control system are frequently done in Matlab/Simulink environment. In this paper, we will demonstrate that there is no need for this control block. Only a simple relation is needed to compute transient duty cycle. Furthermore, the program is realised in terms of a simple and fast Matlab m-file.

According to these goals, the paper is organised as follows. Section 2 develops fundamentals of the inverter. It includes the equivalent electrical circuit modelling the DC-DC boost inverter, commutation equations, properties of DCM and CCM regimes, and dynamical submodels associated with ON and OFF states. Section 3 develops exact and analytical relations of dynamic variables for both ON and OFF states. This section proposes, in particular, a simple correction of the time interval associated with DCM regime. Section 4 deals with fundamental steady-state equations. For both DCM regime and CCM regime, mean values of inductor current and output voltage are detailed and expressed. Effect of inductor inductance, output load resistance, and switching period on the boundary between DCM and CCM is graphically explained. Section 5 presents the main steps of the dynamic simulation algorithm and discusses how to implement the current peak control. In Section 6, we develop the procedure of obtaining a discrete map model and discuss how to conduct the computation of Lyapunov exponents. Finally, Section 7 presents various simulation cases. Results obtained in open-loop and closed-loop control are presented and commented. The discussion is particularly focused on tuning the bifurcation parameter and analysing chaos. Computing time is also considered in the scheme evaluation.

2. Fundamentals of a DC-DC boost inverter

Figure 1 shows an equivalent circuit diagram of a boost DC-DC inverter supplying a pure resistive loadR_o. Parameters$E$, L, and C denote, respectively, the input voltage source, the inductance of the inductor, and the output filtering capacitor. In this work, we consider the most widely used model [2, 8] characterised by ideal components. This means that the power transistor is an ideal switch; the inductor, filtering capacitor, and diode are lossless. In the conduction mode, the voltage across the diode is zero. The power transistor works as short circuit or as an open circuit depending on whenever the signal command $u(t)$ equals 1 or0. Along switching time, boost inverter equivalent circuit shown by Figure 1 takes two forms as shown by Figures 2(a) and Figure 2(b) [14]. During the ON state, the transistor behaves like a short and no current flows through the diode. Therefore, the inductor becomes in fact disconnected from the parallel part $(R_o - C)$ and the positive voltage of the capacitor biases the diode. The current flowing through the inductor increases; as a result, the electromagnetic energy in the inductance L increases. At the same time, the filtering capacitor discharges into the load resistance R_o, and therefore the voltage across the capacitor decreases. During the OFF state, the power transistor behaves like an open circuit, and the diode is conducting. Therefore, the input voltage supplies directly to the load. The voltage across the capacitor increases and the current through the inductor decreases because the electromagnetic energy is transformed into electrostatic energy.

Command $u(t)$ is a PWM signal characterised by a switching period T and a duty cycleα. In the following, this period will be divided into three time intervals t_1, t_2, and t_3 as indicated by equations (1) and (2). The first interval corresponds to the ON state given by $(u(t) = 1)$. The second and third intervals are associated with the OFF state corresponding to $(u(t) = 0)$. In these equations, coefficients (α, β, γ) correspond, respectively, to ratios of (t_1, t_2, t_3) with respect to the switching period$T$. Coefficient $\alpha$is known by duty cycle. Coefficient β is the complement of α in the case of continuous conduction mode (CCM). Coefficient γ is the complement of $(\alpha + \beta)$ in the case of discontinuous conduction mode (DCM).

$$\begin{aligned} t_1 &= \alpha T, \\ t_2 &= \beta T, \\ t_3 &= \gamma T, \end{aligned} \tag{1}$$

$$\begin{aligned} t_1 + t_2 + t_3 &= T, \\ \alpha + \beta + \gamma &= 1. \end{aligned} \tag{2}$$

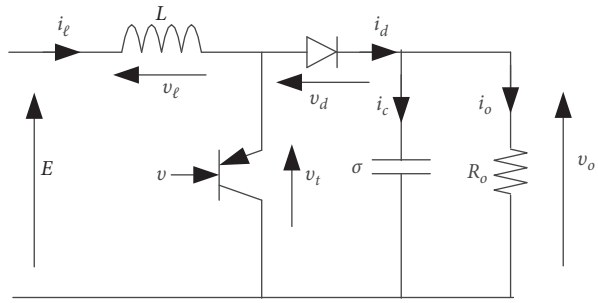

Figure 1: Boost inverter equivalent circuit.

This organisation aims to take into account continuous conduction mode (CCM) and discontinuous conduction mode (DCM) of inductor current. As previously indicated, inductor current $i_\ell(t)$ increases during the ON state and decreases during the OFF state. Let us consider that the switching period T begins with an inductor current $I_{\ell 0}$ and a capacitor voltage V_{c0}, and just when the OFF state takes place, these variables are, respectively, $I_{\ell 1}$and V_{c1}. If $i_\ell(t)$ in the OFF state remains positive until the end of the period, we have the CCM case and $(t_3 = 0)$; therefore, $(t_2 = \beta T = (1-\alpha)T)$. At the end of the period T, the current through the inductor and voltage across the capacitor are denoted $I_{\ell 2}$ and V_{c2}, respectively. If $i_\ell(t)$reaches zero before the period finishes, we have the DCM case, $(t_3 > 0)$ and $(t_2 = \beta T < (1-\alpha)T)$. In this case, the current through the inductor remains null during t_3 because the diode is biased. However, the voltage across the capacitor decreases exponentially from the value V_{c2} to a third value V_{c3}. Figures 3(a) and 3(b) sketch this scenario in terms of inductor current $i_\ell(t)$ and capacitor voltage $v_c(t)$. These figures correspond to the transient regime and report the possible breaking points for a DCM case. For both DCM and CCM regimes, we establish the following commutation equation:

$$\begin{aligned} v_\ell &= E - (1-u)v_o, \\ v_o &= v_c. \end{aligned} \tag{3}$$

Thus, without any particular difficulty, the following dynamic model is derived:

$$\begin{cases} \dfrac{\mathrm{d}i_\ell}{\mathrm{d}t} = \dfrac{E-(1-u)v_c}{L}, \\ \dfrac{\mathrm{d}v_c}{\mathrm{d}t} = \dfrac{(1-u)R_o i_\ell - v_c}{R_o C}. \end{cases} \tag{4}$$

Depending on whether we are dealing with an ON state or an OFF state, we have to treat two different models. In the ON state, the model becomes equivalent to two independent submodels as given by systems (5) and (6). In the OFF state, we have the model given by systems (7) and (8).

$$\begin{cases} \dfrac{\mathrm{d}i_\ell}{\mathrm{d}t} = \dfrac{E}{L}, \end{cases} \tag{5}$$

$$\begin{cases} \dfrac{\mathrm{d}v_c}{\mathrm{d}t} = -\dfrac{v_c}{R_o C}, \end{cases} \tag{6}$$

$$\begin{cases} \dfrac{\mathrm{d}i_\ell}{\mathrm{d}t} = \dfrac{E-v_c}{L}, \end{cases} \tag{7}$$

$$\begin{cases} \dfrac{\mathrm{d}v_c}{\mathrm{d}t} = \dfrac{R_o i_\ell - v_c}{R_o C} \end{cases} \tag{8}$$

For the OFF state case, isolating $v_c$from (7) and establishing its time derivative yields

$$v_c = E - L\frac{\mathrm{d}i_\ell}{\mathrm{d}t}, \tag{9}$$

$$\frac{\mathrm{d}v_c}{\mathrm{d}t} = -L\frac{\mathrm{d}^2 i_\ell}{\mathrm{d}t^2}. \tag{10}$$

Thus, for the OFF state case, equations (9) and (10), combined with equation (8), result in

$$\frac{\mathrm{d}^2 i_\ell}{\mathrm{d}t^2} + \frac{1}{\tau_c}\frac{\mathrm{d}i_\ell}{\mathrm{d}t} + \frac{i_\ell}{\tau_\ell \tau_c} - \frac{I_{er}}{\tau_\ell \tau_c} = 0, \tag{11}$$

$$\begin{aligned} \tau_c &= R_o C, \\ \tau_\ell &= \frac{L}{R_o}, \\ I_{er} &= \frac{E}{R_o}. \end{aligned} \tag{12}$$

The second-order linear ODE (11) furnishes the following characteristic polynomial:

$$s^2 + \frac{s}{\tau_c} + \frac{1}{\tau_\ell \tau_c} = 0. \tag{13}$$

With the condition $(L < 4R_o^2 C)$, this polynomial admits two complex conjugate poles which means that we have a damped oscillating system. The time constant (τ) and the pulsation (ω) are expressed by

$$\begin{aligned} s &= -\frac{1}{\tau} \pm j\omega, \\ \tau &= 2\tau_c = 2R_o C, \\ \omega &= \frac{1}{\tau}\sqrt{\frac{2\tau}{\tau_\ell} - 1}. \end{aligned} \tag{14}$$

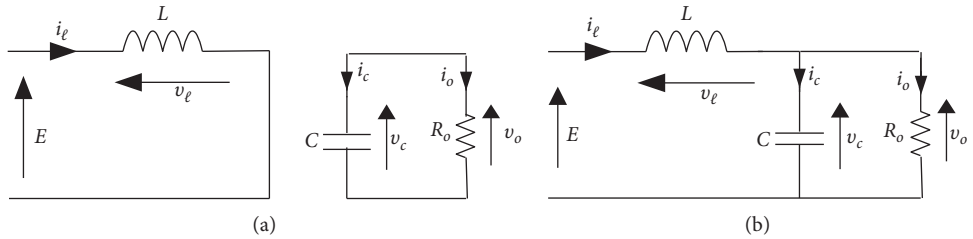

Figure 2: (a) Equivalent circuit in ON state case. (b) Equivalent circuit in OFF state case.

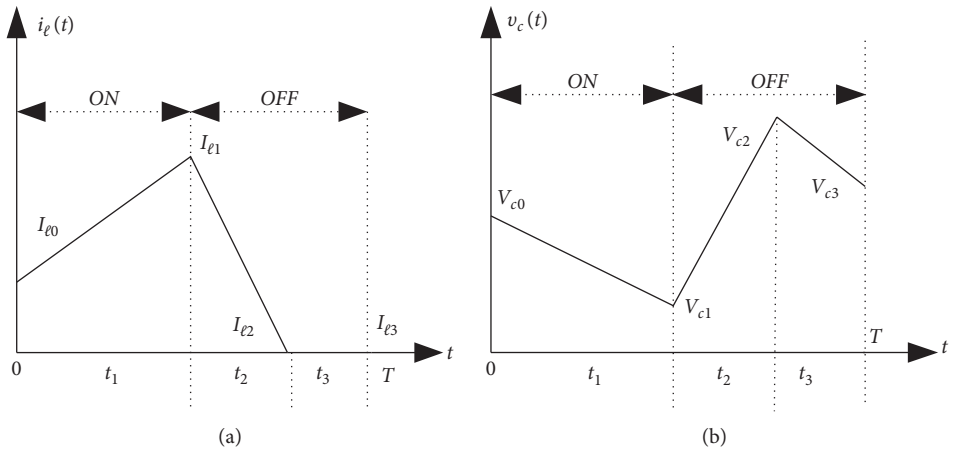

Figure 3: (a) Illustrative evolution of inductor current. (b) Illustrative evolution of capacitor voltage.

3. Temporal Solution of the Mathematical Model

3.1. Analytical Solution of ON State Case. Here, we have to solve a simple dynamic system ((5) and (6)) which is completely decoupled into two independent subsystems. The inductor current and capacitor voltage of the boost inverter are of the form

$$\begin{aligned} i_\ell(t) &= I_{\ell 0} + \frac{E}{L}t, \\ v_c(t) &= V_{c0}e^{-(t/\tau_c)}. \end{aligned} \tag{15}$$

This solution is verified by the construction of $(i_\ell(0) = I_{\ell 0})$ and $(v_c(0) = V_{c0})$. $I_{\ell 1}$ and V_{c1} of $i_\ell(t)$ and $v_c(t)$ at $(t_1 = \alpha T)$ are expressed by

$$\begin{aligned} I_{\ell 1} &= i_\ell(t_1) = I_{\ell 0} + \frac{E\alpha T}{L}, \\ V_{c1} &= v_c(t_1) = V_{c0}e^{-(\alpha T/\tau_c)}. \end{aligned} \tag{16}$$

3.2. Analytical Solution of OFF State Case. Solution $i_\ell(t)$ of (11) is naturally composed of two terms. The first term is the particular solution corresponding to the case where $i_\ell(t)$is constant. The second one is the homogeneous solution which is a sinusoidal damped variable. Thus, we get

$$i_\ell(t) = I_{er} + [\eta_1 \sin(\theta) + \eta_2 \cos(\theta)]e^{-(t/\tau)}, \tag{17}$$

$$\theta = \omega t. \tag{18}$$

For $(t = 0)$, we have $(i_\ell(0) = I_{\ell 1})$ which implies

$$\eta_2 = I_{\ell 1} - I_{er}. \tag{19}$$

To identify parameter η_1, we obtain the derivative with respect to time of equation (17) and make it equal to equation (7). Therefore, we obtain

$$\frac{di_\ell}{dt} = -\left\{\left[\omega\eta_2 + \frac{\eta_1}{\tau}\right]\sin(\theta) + \left[\frac{\eta_2}{\tau} - \omega\eta_1\right]\cos(\theta)\right\}e^{-(t/\tau)} = \frac{E - v_c}{L}. \tag{20}$$

By applying this expression at $(t = 0)$, one deduces

$$\eta_1 = \frac{I_{\ell 1} - I_{er}}{\omega\tau} + \frac{E - V_{c1}}{L\omega}. \tag{21}$$

The behaviour of the voltage across the capacitor is derived from equation (20). This results in

$$v_c(t) = E + [\eta_3 \sin(\theta) + \eta_4 \cos(\theta)]e^{-(t/\tau)}, \tag{22}$$

$$\begin{aligned} \eta_3 &= L\omega\left[\eta_2 + \frac{\eta_1}{\omega\tau}\right], \\ \eta_4 &= L\omega\left[\frac{\eta_2}{\omega\tau} - \eta_1\right]. \end{aligned} \tag{23}$$

To compute values $I_{\ell 2}$ of $i_\ell(t)$ and V_{c2} of $v_c(t)$ at t_2, let us first assume that we are in the CCM regime by setting $(\gamma =$

0) and $(\beta = (1-\alpha))$ or equivalently by setting $(t_3 = 0)$ and $(t_2 = (1-\alpha)T)$. The following equations are obtained. Note that all coefficients $(\eta_1, \eta_3, \eta_4, \eta_5)$are functions of $(\delta = \omega\beta T)$.

$$I_{\ell 2} = I_{er} + \eta_5\left[\eta_1 \sin(\delta) + \eta_2 \cos(\delta)\right], \tag{24}$$

$$V_{c2} = E + \eta_5\left[\eta_3 \sin(\delta) + \eta_4 \cos(\delta)\right], \tag{25}$$

$$\begin{aligned} \eta_5 &= e^{-(\delta/\omega\tau)}, \\ \delta &= \omega\beta T, \\ \beta &= (1-\alpha). \end{aligned} \tag{26}$$

If $I_{\ell 2}$ computed by equation (24) is positive, the assumption of CCM holds and the computed values of $I_{\ell 2}$ and V_{c2} are valid. If $I_{\ell 2}$ is negative, this means that the assumption is false and we are in DCM case. Consequently, coefficient β is less than $(1-\alpha)$ and must be equal to the solution satisfying

$$I_{\ell 2} = I_{er} + \eta_5(\delta)\left[\eta_1(\delta)\sin(\delta) + \eta_2 \cos(\delta)\right] = 0. \tag{27}$$

This relation is nonlinear in terms of β and needs to be solved iteratively by the Newton–Raphson method. To ovoid additional computing time, we propose to compute β by linearizing $i_\ell(t)$ around $(t = 0)$ and setting the result to zero. This approach is based on the fact that the damping time constant (τ) is big enough when compared with the switching period, which is true in the real world. So, applying a first-order Taylor expansion to equation (20) yields

$$\begin{aligned} i_\ell(t) &= I_{\ell 1} + \frac{\mathrm{d}i_\ell}{\mathrm{d}t}\Big|_{t=0}, \\ t &= I_{\ell 1} - \left[\frac{V_{c1} - E}{L}\right]t. \end{aligned} \tag{28}$$

Thus, we obtain

$$\beta = \frac{LI_{\ell 1}}{(V_{c1} - E)T}. \tag{29}$$

The voltage of the capacitor V_{c2} at $(t_2 = \beta T)$ is recomputed by using equation (25) that continues to be valid with the new value of $(\beta < (1-\alpha))$. During the remaining time interval $(t \in [(\alpha+\beta)TT])$, the inductor current is kept null; $(i_\ell(t) = I_{\ell 2} = 0)$. However, the voltage across the capacitor decreases exponentially from the value V_{c2} to a third valueV_{c3}. At the end of the switching period, this voltage takes the value of

$$\begin{aligned} V_{c3} &= V_{c2}e^{-(\gamma T/\tau)}, \\ \gamma &= 1 - \alpha - \beta. \end{aligned} \tag{30}$$

Note finally that according to Figures 3(a) and 3(b), the mean values of the current through the inductor and the voltage of the capacitor are calculated at each switching period by the following equations. In the case of CCM, the third term in equation (31) must be removed because $\gamma$is null in this situation.

$$I_\ell = \frac{\alpha(I_{\ell 0} + I_{\ell 1}) + \beta(I_{\ell 1} + I_{\ell 2})}{2}, \tag{31}$$

$$V_c = \frac{\alpha(V_{c0} + V_{c1}) + \beta(V_{c1} + V_{c2}) + \gamma(V_{c2} + V_{c3})}{2}. \tag{32}$$

4. Fundamental Steady-State Equations

As previously outlined, there are two possible modes for the boost converter: CCM and DCM. In CCM, the inductor current flows continuously above zero during the totality of the switching period. The output voltage can be described by a relatively simple expression making control reliable via the duty cycleα. In addition, the inductor voltage waveform is almost a constant signal that results in an inductor current ripple close to a triangular signal. In the DCM, the inductor current reaches zero before the end of the switching period. The output voltage is described by a high nonlinear equation in terms of the duty cycle making it difficult to control. Figures 4(a) and 4(b) sketch general shapes of the inductor and diode current in the case of DCM regime.

To evaluate the input current and the output voltage in steady operating conditions, we use the small ripple approximation hypothesis that permits to replace instantaneous variables in minor time intervals by their mean values. Figures 5(a) and 5(b) report waveforms of inductor voltage $v_\ell(t)$ and capacitor current $i_c(t)$ during one switching period. During the three possible time intervals forming the switching period as defined by Figures 3(a) and 3(b), from Figures 5(a) and 5(b), we establish

$$\begin{aligned} &t \in t_1 = \alpha T\colon V_\ell = E, I_c = -\frac{V_o}{R_o} = -I_o, \\ &t \in t_2 = \beta T\colon V_\ell = E - V_o, I_c = I_\ell - I_o, \\ &t \in t_3 = \gamma T\colon V_\ell = 0, I_c = -I_o. \end{aligned} \tag{33}$$

By applying the principle of charge-discharge balance of inductor electromagnetic energy and capacitor electrostatic energy, mean values $V_\ell$and I_c of $v_\ell(t)$ and $i_c(t)$ must be zero. So, we deduce

$$\begin{aligned} \alpha E + \beta(E - V_o) &= 0, \\ -(1-\beta)I_o + \beta(I_\ell - I_o) &= 0. \end{aligned} \tag{34}$$

Solving these equations for unknown V_o andI_ℓ, we generate the steady-state solution:

$$V_o = \frac{(\alpha+\beta)E}{\beta}, \tag{35}$$

$$I_\ell = \frac{I_o}{\beta} = \frac{(\alpha+\beta)I_{er}}{\beta^2}. \tag{36}$$

Also, note that equations (35) and (36) established above for steady state of CCM case can be found from models (5) and (6) if we substitute variable $(1-u)$ by its mean value

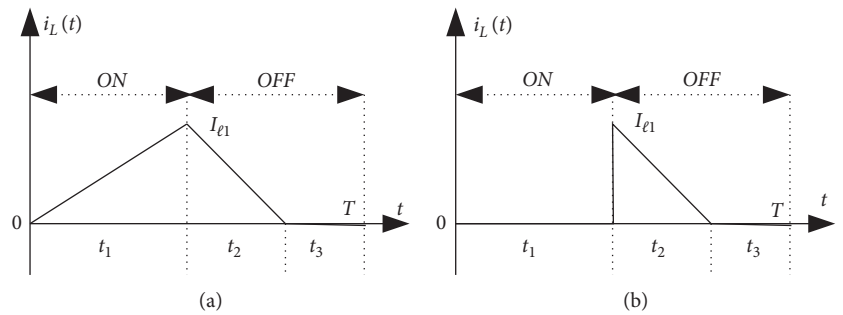

Figure 4: (a) General shape of inductor current in DCM. (b) General shape of diode current in DCM.

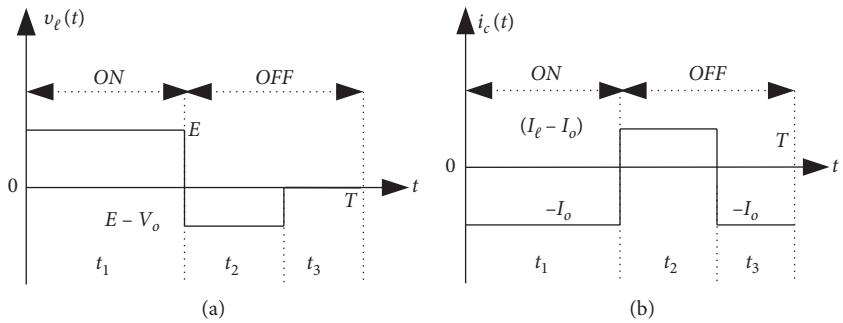

Figure 5: (a) Simplified waveform of inductor voltage. (b) Simplified waveform of capacitor current.

$\beta$and we set time derivatives to zero as in classical continuous dynamic systems.

4.1. Continuous Conduction Mode. In the CCM case, we have $(\beta = (1 - \alpha))$, and consequently equations (35) and (36) become

$$V_o = \frac{E}{1 - \alpha}, \tag{37}$$

$$I_\ell = \frac{I_{er}}{(1 - \alpha)^2}. \tag{38}$$

With this assumption, the peak-to-peak ripple of the inductor current and capacitor voltage is approximated by the following equations:

$$\Delta i_\ell \simeq \frac{E\alpha T}{L}, \tag{39}$$

$$\Delta v_C \simeq \frac{I_{er}\alpha T}{C(1 - \alpha)}. \tag{40}$$

4.2. Discontinuous Conduction Mode. In the DCM case, the initial inductor current $I_{\ell 0}$ is zero and peak current $I_{\ell 1}$ is such that

$$I_{\ell 1} = \frac{E\alpha T}{L}. \tag{41}$$

The inductor peak current $I_{\ell 1}$ and diode average current I_d are defined by

$$I_d = I_o = \frac{\beta I_{\ell 1}}{2} = \frac{\beta E\alpha T}{2L}. \tag{42}$$

This allows us to deduce

$$\beta = \frac{KV_o}{\alpha E}, \qquad K = \frac{2L}{R_o T}. \tag{43}$$

Substituting β into equation (35) results in

$$KV_o(V_o - E) - (\alpha E)^2 = 0. \tag{44}$$

Solving equation (44) in terms of V_o allows us to define the output voltage and input current:

$$V_o = \frac{E}{2}\left[1 + \sqrt{1 + \frac{4\alpha^2}{K}}\right], \tag{45}$$

$$I_\ell = \frac{\left(E\alpha^2 + KV_o\right)}{R_o K}. \tag{46}$$

Just when the steady-state operating point passes from the CCM to the DCM regime, i.e., just at the boundary separating these regimes, the voltage solution given by equation (45) becomes greater than that of equation (35). That is:

$$1+\sqrt{1+\frac{4\alpha^2}{K}}>\frac{2}{1-\alpha}. \quad (47)$$

Arranging this, one concludes that DCM is characterised by the following inequality:

$$f(\alpha)=\alpha(1-\alpha)^2>K. \quad (48)$$

Function $f(\alpha)$ of inequality (48) passes by a maximum point defined by $(f_{\max}=4/27)$ for $(\alpha=1/3)$ as illustrated by Figure 6. If $(K\geq f_{\max})$, the inductor current is continuous over the complete range of the switching period and relations (37) and (38) hold for $(\alpha\in[\,0\ \ 1\,])$. If $(K<f_{\max})$, the inductor current has a discontinuous mode in the interval $(\alpha\in[\,\alpha_1\ \ \alpha_1\,])$ and a continuous mode in the remaining intervals $(\alpha\in[\,0\ \ \alpha_1\,])$ and $(\alpha\in[\,\alpha_2\ \ 1\,])$. Parameters $\alpha_1$and α_2 are the solutions of equation $(f(\alpha)=K)$. In the central region where we have DCM, the output voltage and input current are given by equations (45) and (46).

5. Dynamic Simulation Algorithm and Control

Now that all necessary relations to realise the dynamic simulation of the boost converter are available, it is of importance to note that an integration step that corresponds to a one switching period is needed. We will first present how the integration process works. Second, we will discuss the possibility of implementation of the classical switching controller.

5.1. Dynamic Simulation Algorithm. The dynamic simulation algorithm is simple. It is based on the following main steps:

(i) Set the initial inductor current and capacitor voltage $(i_\ell=I_{\ell 0}=0)$ and $(v_c=V_{c0}=0)$ and save these values as a first point.

(ii) Compute $(I_{\ell 1},V_{c1})$ and save this point.

(iii) Compute $(I_{\ell 2},V_{c2})$ using $(\beta=1-\alpha)$. If $(I_{\ell 2}\geq 0)$, save this point and go to step (iv); otherwise, go to step (v).

(iv) Reinitialise with $(I_{\ell 0}=I_{\ell 2})$ and $(V_{c0}=V_{c2})$ and go to step (ii).

(v) Recompute β and V_{c2} as previously explained and save the new point $(0,V_{c2})$. Then, compute V_{c3}, set $(I_{\ell 3}=0)$, and save this point.

(vi) Reinitialise with $(I_{\ell 0}=0)$ and $(V_{c0}=V_{c3})$ and go to step (ii).

It is obvious that for one period, we have to save two or three points depending on whether we are in the CCM or DCM case. Furthermore, if we zoom in a plotted curve illustrating the result, we find a linear piecewise trajectory. The reason is evident.

5.2. Dynamic Control. Various interesting works in the field of control design of DC-DC boost inverter, such as classical control [8], sliding mode control [17], fuzzy control [18], and so on, can be found in the literature. Widely used approaches develop a second-order controller based on transfer functions for small signals. Here, the main goal is to implement the classical switching controller, which is by nature a current peak controller (CPC). The feedback control block is composed of a saw tooth generator, a comparator, and a latch. The output of the latch is used by the drive circuit that generates the gating pulses. The switch is turned on at the beginning of each switching period and turned off if the inductor current becomes greater than a programmed reference value I_{ref} and remains in the OFF state until the beginning of the next cycle. During simulation, this is equivalent to computing the PWM duty cycle α from the initial current $I_{\ell 0}$ and reference current I_{ref}. Thus, at the beginning of the period, duty cycle α is computed by equation (49) which is equivalent to equation (41) where $I_{\ell 1}$ is set equal to I_{ref}. The simulation algorithm previously presented remains practically the same.

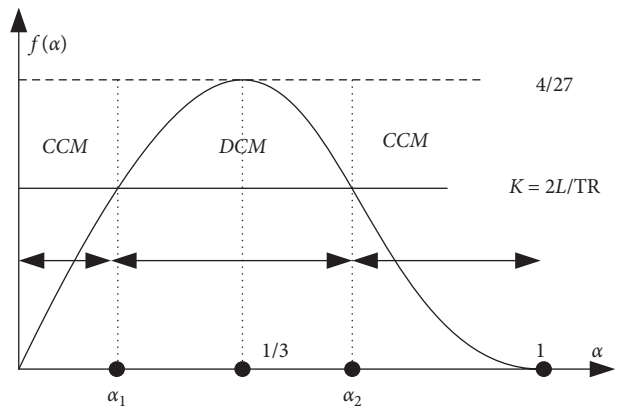

Figure 6: DCM-CCM boost inverter curve.

$$\alpha=\frac{(I_{\text{ref}}-I_{\ell 0})L}{TE}. \quad (49)$$

6. Discrete Map and Lyapunov Exponents of DC-DC boost inverter

In this section of the paper, the load resistance is chosen to ensure that the circuit operates theoretically in the continuous mode. The sequence of the braking points computed for a set of some consecutive switching periods is used to define a discrete iterative map process. The obtained time series added to the Jacobian matrix of the map permits the computation of Lyapunov exponents. If the largest Lyapunov exponent (LLE) is positive, the system enters in a chaotic behaviour. Points corresponding to the minimum peak current form the selected discrete time series. In this sense, let us indicate two successive switching periods by $(k,k+1)$ and denote the couple $(I_{\ell 0},I_{\ell 2})$ of inductor current and the corresponding couple (V_{c0},V_{c2}) of voltage capacitor as follows:

$$\begin{aligned} I_{\ell 0} &= x_k, \\ I_{\ell 2} &= x_{k+1}, \\ V_{c0} &= y_k, \\ V_{c2} &= y_{k+1}. \end{aligned} \tag{50}$$

In this way, equation (50) of the duty cycle and equations (21), (23), and (26) of coefficients $(\eta_1, \eta_3, \eta_4, \eta_5)$ are reformulated as functions of the discrete iterative variables.

$$\begin{aligned} \delta &= \delta(x_k) = \omega T - \frac{L\omega}{E}(I_{\text{ref}} - x_k), \\ \eta_0 &= \eta_0(x_k) = e^{-(2(\omega T - \delta(x_k))/\omega\tau)}, \\ \eta_1 &= \eta_1(x_k, y_k) = \frac{\eta_2}{\omega\tau} + \frac{E - \eta_0(x_k) y_k}{L\omega}, \\ \eta_3 &= \eta_3(x_k, y_k) = L\omega\left[\eta_2 + \frac{\eta_1(x_k, y_k)}{\omega\tau}\right], \\ \eta_4 &= \eta_4(x_k, y_k) = L\omega\left[\frac{\eta_2}{\omega\tau} - \eta_1(x_k, y_k)\right], \\ \eta_5 &= \eta_5(x_k) = e^{-(\delta(x_k)/\omega\tau)}. \end{aligned} \tag{51}$$

This leads to the iterative process defined by

$$\delta(x_k) = \omega T - \frac{L\omega}{E}(I_{\text{ref}} - x_k), \tag{52}$$

$$\begin{aligned} f_x(x_k, y_k) = I_{er} + \eta_5(x_k)[\eta_1(x_k, y_k)\sin(\delta(x_k)) \\ + \eta_2 \cos(\delta(x_k))], \end{aligned} \tag{53}$$

$$\begin{aligned} f_y(x_k, y_k) &= E + \eta_5(x_k)[\eta_3(x_k, y_k)\sin(\delta(x_k)) \\ &\quad + \eta_4(x_k, y_k)\cos(\delta(x_k))], \\ x_{k+1} &= f_x(x_k, y_k), \\ y_{k+1} &= f_y(x_k, y_k). \end{aligned} \tag{54}$$

Let $J(x, y)$ denote the Jacobian matrix associated with the system above. The computation of this matrix at each iteration furnishes the possibility to compute Lyapunov exponents λ via the QR factorisation method. This is the most suitable method to compute these exponents for a time series process with known Jacobian. At each iteration k, the Lyapunov exponents are computed as follows:

$$\lambda(k) = \frac{1}{k}\sum_{k} \text{Log}(|\text{Diag}(R)|). \tag{55}$$

In this relation, $\text{Diag}(R)$ denotes the diagonal of matrix R computed in Matlab environment by the following syntax. In this process, matrix Q is initialised by the identity matrix. Note also that because $J(x, y)$ is space consuming, the development of its elements is reported in the Appendix.

$$[Q, R]_{k+1} = qr(J_k Q_k). \tag{56}$$

Kaplan–Yorke dimension [19] is a powerful tool that describes the complexity of chaotic attractors. This dimension is also known by the Kaplan–Yorke conjecture. First, Lyapunov exponents are arranged in decreasing order $(\lambda_1 > \lambda_2 > \cdots \lambda_n)$, and index j corresponding to inequality (57) is determined. Then, the conjecture is that the dimension of the attractor is given by (53). For the studied case, equation (58) is equivalent to equation (59).

$$\begin{aligned} \sum_{i=1}^{j} \lambda_j \geq 0, \\ \sum_{i=1}^{j+1} \lambda_j < 0, \end{aligned} \tag{57}$$

$$D_{ky} = j + \frac{1}{|\lambda_{j+1}|}\sum_{i=1}^{j} \lambda_i, \tag{58}$$

$$D_{ky} = 1 + \frac{\lambda_1}{|\lambda_2|}. \tag{59}$$

Reference peak current I_{ref} will be considered a bifurcation parameter. By varying I_{ref}, we will observe how the circuit changes its behaviour from a stable system to a chaotic system via the period-doubling mechanism.

7. Results and Comments

The boost inverter parameters used to illustrate this study are reported in Table 1. Results are carried out in Matlab environment. Necessary software is written in a m-file code. For all simulations, the initial inductor current and capacitor voltage are set to zero.

According to these parameters, the frequency and time constant characterising dynamic inverter behaviour in the OFF state are $(f = 1.415\,\text{kHz})$ and $(\tau = 480\,\mu\text{s})$, respectively. This time constant is 4.8 times greater than the switching period. Equation (48) implies that the DCM boundary coefficient is $(K = 1 > 4/27)$. That is, the inverter works in CCM for full range of the duty cycle because the used rated resistance load is less than the critical load resistance whose value is $(R_o = 135\,\Omega)$. To simulate a DCM case, we use $(R_o = 200\,\Omega)$. In this case, we have $(K = 0.1 < 4/27)$ that results in a DCM in the range $(\alpha \in [\,0.1330 \;\; 0.5874\,])$.

7.1. Simulation No. 1. Two simulation tests are carried out. The first test corresponds to $(\alpha = 0.5)$ and $(R_o = 20\,\Omega)$. A CCM regime is expected. Using equation (38), we found $(I_\ell = 1.967\,\text{A})$. The second simulation is realised with $(\alpha = 0.3)$ and $(R_o = 200\,\Omega)$ and a DCM regime is expected. Using equation (46), we found $(I_\ell = 0.1237\,\text{A})$. Figures 7(a) and 7(b) show steady-state evolution of inductor current for these tests, respectively, and confirm the predicted $I_\ell$values.

Table 1: System parameters.

Parameter	Notation	Value
Rated input voltage	E	10 V
Rated resistance of the load	R_o	20 Ω
Rated switching period	T	100 μs
Inductor inductance	L	1000 μH
Filtering capacitor	C	12 μF

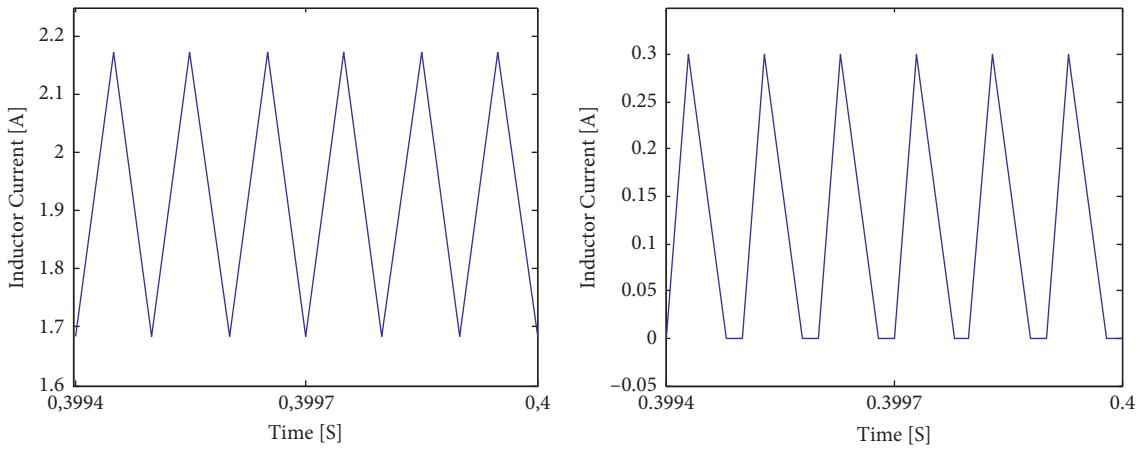

Figure 7: (a) CCM steady state of inductor current in open-loop case. (b) DCM steady state of inductor current in open-loop case.

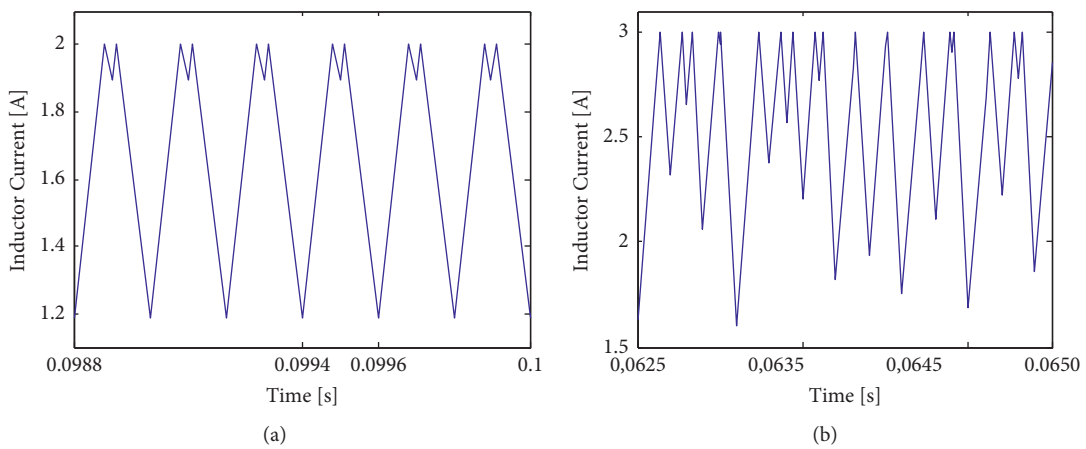

Figure 8: (a) CCM chaotic steady state of inductor current in closed-loop test with ($I_{\text{ref}} = 2$ A). (b) CCM chaotic steady state of inductor current in closed-loop test with ($I_{\text{ref}} = 3$ A).

7.2. Simulation No. 2. We consider a load resistance ($R_o = 20\,\Omega$), and we simulate two tests of inductor current peak: ($I_{\text{ref}1} = 2$ A) and ($I_{\text{ref}2} = 3$ A). Figures 8(a) and 8(b) show steady-state evolution of inductor current for these two tests, respectively. $I_{\ell 2}$ and V_{c2} of inductor current and capacitor voltage at the end of the switching period are saved. Figures 9(a) and 9(b) show phase portraits of $I_{\ell 2}$ and V_{c2} in dot plot form. Figures 10(a) and 10(b) show the dot plot of ($I_{\ell 2} = f(\alpha)$) and ($V_{c2} = f(\alpha)$), respectively. All these figures show without ambiguity the existence of chaos phenomenon in boost DC-DC dynamics when controlled in CPC type. To show areas with period doubling and those of intermittence, a fine variation of bifurcation parameter is required.

7.3. Simulation No. 3. The load resistance ($R_o = 20\,\Omega$) is used. We tune the bifurcation parameter I_{ref} with a small variation in the range of 1 A to 5 A. For each value of I_{ref}, we discard the transient part of the trajectory and save the remaining steady-state part. At the end, all results are plotted in dot plot form. Lyapunov exponents are calculated at the same time of dynamic trajectories. Figures 11(a) and 11(b) show bifurcation diagrams of inductor current and capacitor

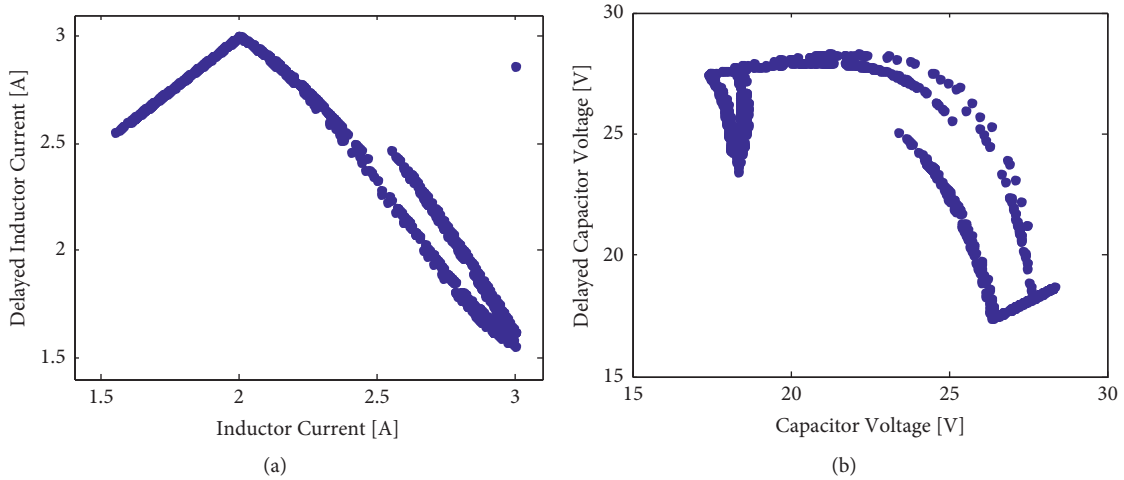

FIGURE 9: (a) Phase portrait of CCM chaotic steady state of inductor current in closed-loop test with (I_{ref} = 3 A). (b) Phase portrait of CCM chaotic steady state of voltage capacitor in closed-loop test with (I_{ref} = 3 A).

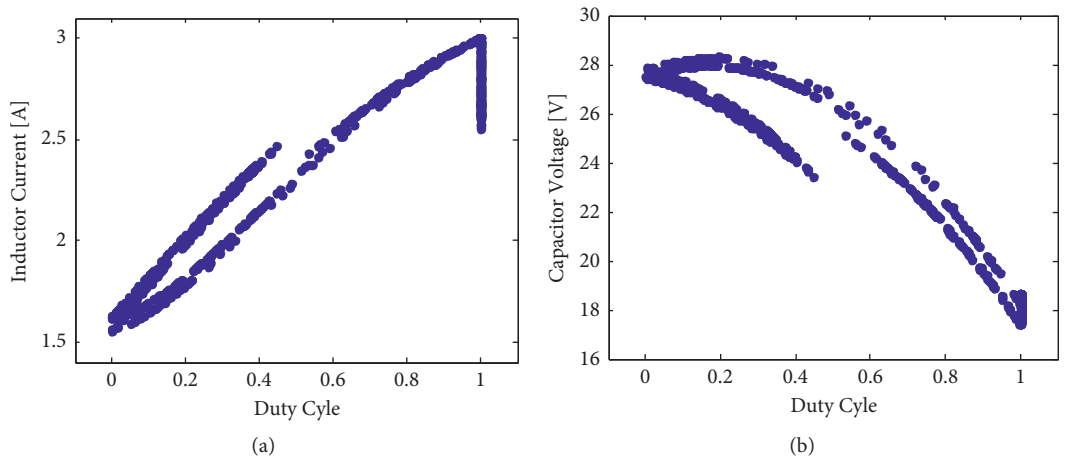

FIGURE 10: (a) Closed-loop CCM chaotic steady state of inductor current versus duty cycle (I_{ref} = 3 A). (b) Closed-loop CCM chaotic steady state of capacitor voltage versus duty cycle (I_{ref} = 3 A).

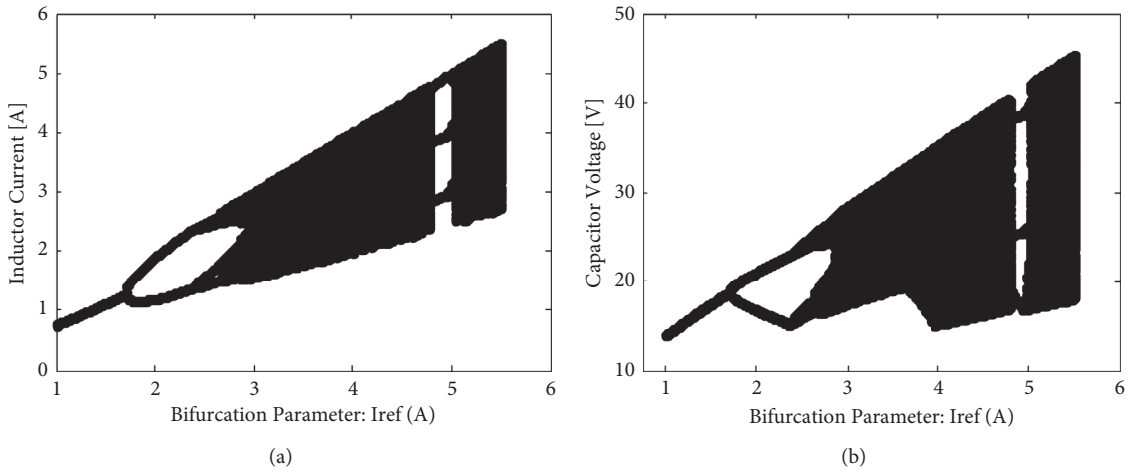

FIGURE 11: (a) Bifurcation diagram of inductor current. (b) Bifurcation diagram of capacitor voltage.

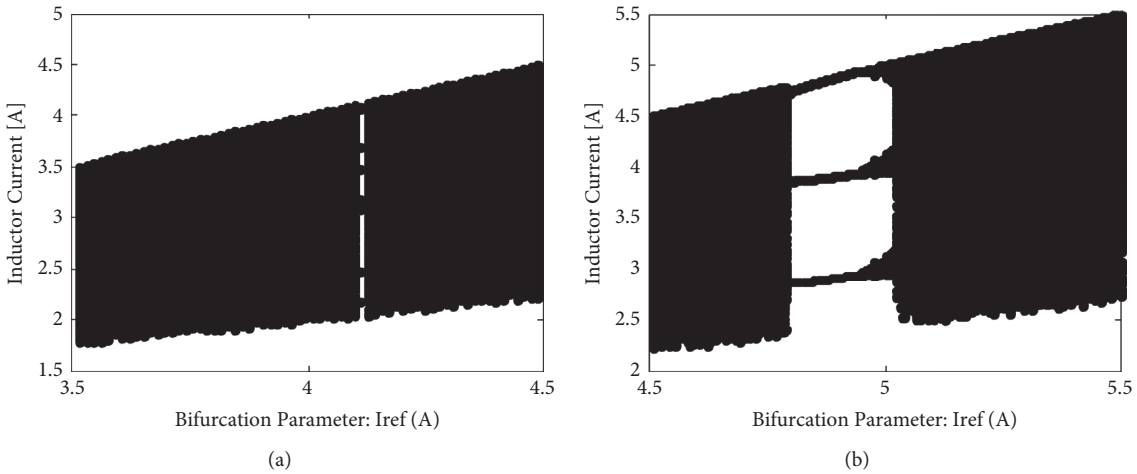

FIGURE 12: (a) First zoom on bifurcation diagram of inductor current. (b) Second zoom on bifurcation diagram of inductor current.

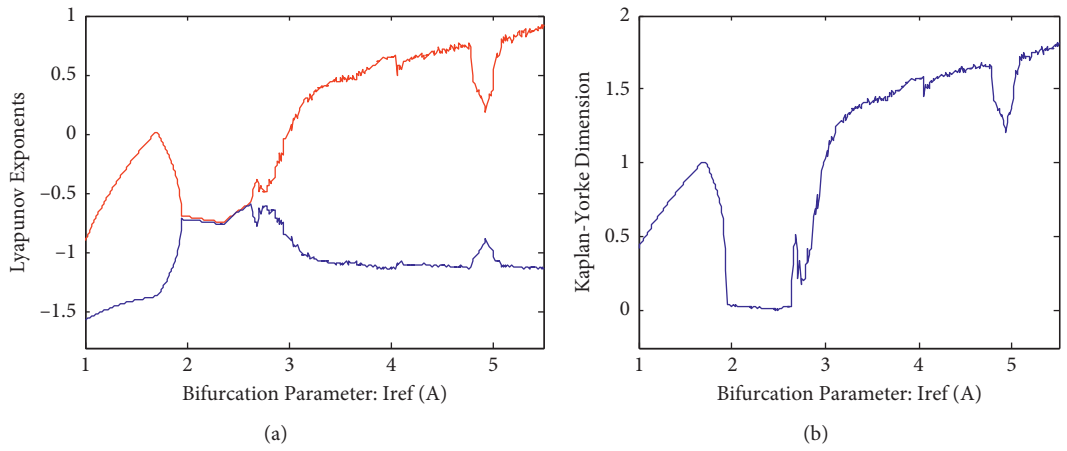

FIGURE 13: (a) Effect of bifurcation parameter on Lyapunov exponents. (b) Effect of bifurcation parameter on Kaplan–Yorke dimension.

voltage, respectively. We observe the phenomenon of period doubling and then the entrance of the system in a chaotic behaviour. Figures 12(a) and 12(b) furnish more details on this behaviour. It is observed that period doubling begins with ($I_{\text{ref}} = 1.69$ A). Then, at ($I_{\text{ref}} = 2.37$ A), ($I_{\text{ref}} = 2.63$ A), and ($I_{\text{ref}} = 2.7$ A), the system enters in $4T$, $8T$, and $16T$ type orbits, respectively. Two intermittence [20] areas are observed around ($I_{\text{ref}} = 4.1$ A) and ($I_{\text{ref}} = 4.9$ A). Figures 13(a) and 13(b) show Lyapunov exponents and Kaplan–Yorke dimension evolution versus the bifurcation parameter. As the system is of dimension 2, we generate two Lyapunov exponents. It is found that one (LLE) becomes positive for a bifurcation parameter ($I_{\text{ref}} > 2.8$ A). This indicates the beginning of a chaotic region. The second exponent is negative. The largest exponent is red colored while the other is blue colored. Note that LLE detects intermittence areas. Kaplan–Yorke dimension evolution is similar to LLE because LLE here is dominant. In the chaotic region, this dimension increases but remains inferior to 2, the physical dimension of the system.

8. Conclusion

We have developed in this paper a study on DC-DC boost inverter based on two levels. The first level of the paper develops a like-discrete integration process based on determination of precise analytical relations of breaking points characterising the switching behaviour of DC-DC boost inverter. The presented scheme gives good results in a very fast manner because for one switching period, we compute only two three breaking points depending on whether we have a continuous conduction mode (CCM) or a discontinuous conduction mode (DCM) of the inductor current. Performance of the developed analytical solution is thus successfully proved. The second level of the paper develops a discrete iterative map as in standard discrete time series models. Jacobian matrix of the found iterative map is defined and used to compute Lyapunov exponents. These exponents confirm the existence of chaos in the system behaviour when varying the reference value of the controlled inductor current. This level of the study is limited to CCM regime. On

the other hand, it is obvious that established iterative map can be easily extended to other inverter topologies such as interleaved configurations [21].

Appendix

A. Jacobian Matrix of the Discrete Iterative Map

First, compute these preliminary coefficients:

$$\begin{aligned}
\frac{\partial \delta}{\partial x} &= \frac{L\omega}{E},\\
\frac{\partial \eta_0}{\partial \delta} &= \frac{2\eta_0}{\omega T},\\
\frac{\partial \eta_1}{\partial \delta} &= -\frac{Y}{L\omega}\frac{\partial \eta_0}{\partial \delta},\\
\frac{\partial \eta_1}{\partial x} &= \frac{\partial \eta_1}{\partial \delta}\frac{\partial \delta}{\partial x},\\
\frac{\partial \eta_1}{\partial y} &= -\frac{\eta_0}{L\omega},\\
\frac{\partial \eta_3}{\partial x} &= \frac{L}{\tau}\frac{\partial \eta_1}{\partial x},\\
\frac{\partial \eta_3}{\partial y} &= \frac{L}{\tau}\frac{\partial \eta_1}{\partial y},\\
\frac{\partial \eta_4}{\partial x} &= -\omega L\frac{\partial \eta_1}{\partial x},\\
\frac{\partial \eta_4}{\partial y} &= -\omega L\frac{\partial \eta_1}{\partial y},\\
\frac{\partial \eta_5}{\partial \delta} &= -\frac{\eta_5}{\omega \tau},\\
\frac{\partial \eta_5}{\partial x} &= \frac{\partial \eta_5}{\partial \delta}\frac{\partial \delta}{\partial x}.
\end{aligned} \tag{A.1}$$

Secondly, compute the Jacobian matrix by

$$J(x,y) = \begin{bmatrix} \frac{\partial f_x}{\partial x} & \frac{\partial f_x}{\partial y} \\ \frac{\partial f_y}{\partial x} & \frac{\partial f_y}{\partial y} \end{bmatrix} = \begin{bmatrix} J_{11} & J_{12} \\ J_{21} & J_{22} \end{bmatrix},$$

$$\begin{aligned}
J_{11} &= \frac{\partial F_x}{\partial x} = \left[\eta_1 \sin(\delta) + \eta_2 \cos(\delta)\right]\frac{\partial \eta_5}{\partial x} + \eta_5\frac{\partial \eta_1}{\partial x}\sin(\delta)\\
&\quad + \eta_5\left[\eta_1 \cos(\delta) - \eta_2 \sin(\delta)\right]\frac{\partial \delta}{\partial x},\\
J_{12} &= \frac{\partial F_x}{\partial y} = \eta_5\frac{\partial \eta_1}{\partial y}\sin(\delta),\\
J_{21} &= \frac{\partial F_y}{\partial x} = \left[\eta_3 \sin(\delta) + \eta_4 \cos(\delta)\right]\frac{\partial \eta_5}{\partial x}\\
&\quad + \eta_5\left[\eta_3 \cos(\delta) - \eta_4 \sin(\delta)\right]\frac{\partial \delta}{\partial x}\\
&\quad + \eta_5\left[\frac{\partial \eta_3}{\partial x}\sin(\delta) + \frac{\partial \eta_4}{\partial x}\cos(\delta)\right],\\
J_{22} &= \frac{\partial F_y}{\partial y} = \eta_5\left[\frac{\partial \eta_3}{\partial y}\sin(\delta) + \frac{\partial \eta_4}{\partial y}\cos(\delta)\right].
\end{aligned} \tag{A.2}$$

Data Availability

The parameters of DC-DC boost converter used to support the findings of this study are included within the article.

Conflicts of Interest

The authors declare that they have no conflicts of interest.

References

[1] K. De Gusseme, M. David, S. Van de, P. Alex, B. Van den, and A. M. Jan, "Digital control of boost PFC converters operating in both continuous and discontinuous conduction mode," in *Proceedings of the 35th Annual IEEE Power Electronics Specialists Conference Aachen*, Aachen, Germany, June 2004.

[2] W. Jiang, Y.-f. Zhou, and J.-n. Chen, "Modelling and simulation of boost converter in CCM and DCM," in *Proceedings of the 2nd International Conference on Power Electronics and Intelligent Transportation System*, Shenzhen, China, November 2009.

[3] T. Suntio, "Modelling and analysis of a PCM-controlled boost converter designed to operate in," *DCM' Energies*, vol. 12, p. 4, 2019.

[4] E. N. Chaves, G. P. Viajante, M. A. A. Freitas et al., "Design based on internal model applied in a quadratic boost converter with P&O MPPT," in *Proceedings of the International Conference on Renewable Energies and Power Quality (ICREPQ'18)*, Salamanca, Spain, March 2018.

[5] V. García-Rodríguez, R. Silva-Ortigoza, E. Hernández-Márquez, J. García-Sánchez, and H. Taud, "DC/DC boost converter-inverter as driver for a DC motor: modeling and experimental verification," *Energies*, vol. 11, no. 8, p. 2044, 2018.

[6] P. Karamanakos, T. Geyer, and S. Manias, "Direct voltage control of DC-DC boost converters using model predictive control based on enumeration," in *Proceedings of the 15th International Power Electronics and Motion Control Conference, EPE-PEMC 2012 ECCE Europe*, Novi Sad, Serbia, September 2012.

[7] J. Moreno-Valenzuela and O. Garcia-Alarcon, "On control of a boost DC-DC power converter under constrained input," *Complexity*, vol. 2017, Article ID 4143901, , 2019.

[8] R. De Keyser, J. Bonilla, and C. Ionescu, "A comparative study of several control techniques applied to a boost converter," in *Proceedings of the IEEE 10th International Conference on*

Optimisation of Electrical and Electronic Equipment OPTIM, Brasov, Romania, December 2006.

[9] F. H. Qi and Y. Sun, "Study of bifurcation and chaos in the current-mode controlled boost DC-DC converter," *Applied Mechanics and Materials*, vol. 733, pp. 635–638, 2015.

[10] M. Jayakumar and V. Vanitha, "Investigation of chaos and bifurcation in boost converter," *International Journal of Pure and Applied Mathematics*, vol. 18, no. 11, pp. 171–177, 2018.

[11] B.-C. Bao, J.-P. Xu, and Y. Liang, "Inductor current sampled feedback control of chaos in current-mode boost converter," *Journal of Electronic Science and Technology of China*, vol. 6, no. 1, 2008.

[12] O. Boubaker and R. Dhifaoui, "Robust chaos synchronisation for Chua's circuits via active sliding mode control," in *Chaos, Complexity and Leadership*, S. Banerjee and S. S. Ercetin, Eds., Springer, Berlin, Germany, 2012.

[13] A. Lassoued, O. Boubaker, R. Dhifaoui, and S. Safari, "Experimental observations and circuit realization of a Jerk chaotic system with piecewise nonlinear function," *Recent Advances in Chaotic Systems and Synchronization*, Elsevier Inc, Amsterdam, Netherlands, 2019.

[14] D. Tannir, Y. Wang, and P. Li, "Accurate modelling of non ideal low-power PWM DC-DC converters operating in CCM and DCM using enhanced circuit-averaging techniques," *ACM Transactions on Design Automation of Electronic Systems*, vol. 21, no. 4, Article ID 61, 2016.

[15] W. Alan, B. Jack, L. S. Harry, and A.V. John, "Determining Lyapunov exponents from a time series," *Physica 16D*, pp. 285–317, North-Holland, Amsterdam, Netherlands, 1985.

[16] L. A. Dmitrieva, Y. A. Kuperin, N. M. Smetanin, and A.C. German, "Method of calculating Lyapunov exponents for time series using artificial neural networks committees," in *Proceedings of the International Conference Days on Diffraction*, pp. 127–132, St. Petersburg, Russia, July 2016.

[17] H. Guldemir, "Modelling and sliding mode control of Dc-Dc buck-boost converter," in *Proceedings of the 6th International Advanced Technologies Symposium (IATS'11)*, Elazıg, Turkey, May 2011.

[18] R. Bazdaric, M. Drago, A. Leban, D. Voncina, and I. Skrjanc, "Fuzzy model predictive control of a DC-DC boost converter based on non-linear model identification," *Mathematical and Computer Modelling of Dynamical Systems*, vol. 23, 2016.

[19] J. L. Kaplan and J. A. Yorke, "Chaotic behavior of multidimensional difference equations," in *Functional Differential Equations and Approximations of Fixed Points*, H.-O. Peitgen and H.-O. Walther, Eds., Springer-Verlag, Berlin, Germany, 1979.

[20] Y. Zhou, J. Ning, H. C. Herbert, and K. Chi, "Complex intermittency in switching converters," *International Journal of Bifurcation and Chaos*, vol. 18, no. 1, pp. 121–140, 2008.

[21] M. Kabalo, D. Paire, B. Blunier, D. Bouquain, M. Godoy Simões, and A. Miraoui, "Experimental evaluation of four-phase floating interleaved boost converter design and control for fuel cell applications," *IET Power Electronics*, vol. 6, no. 2, pp. 215–226, 2013.